J. Numer. Math., Vol. 10, No. 2, pp. 127–136 (2002)

A combined spectral element/finite element approach to the numerical solution of a nonlinear evolution equation describing amorphous surface growth of thin films

R. H. W. HOPPE* and E. M. NASH*

Received 11 March, 2002

Abstract — We consider a nonlinear parabolic PDE that describes the evolution of the surface morphology in the deposition of thin glassy films by molecular beam epitaxy. Due to the dynamics of the growth process which exhibits some unexpected initial linear behavior, for the numerical solution we suggest a combined spectral element/finite element approach. The results of numerical simulations are in good agreement with experimental measurements and show a superior performance of the chosen method compared to more traditional techniques.

Keywords: amorphous surface growth, deposition of thin films, nonlinear evolution equation, spectral elements, finite elements

1. INTRODUCTION

The production of thin glassy films like ZrAlCu by molecular beam epitaxy reveals an amorphous growth of the surface with micro structures that significantly change their shape during the process. The surface morphology exhibits mesa like structures whose magnitude grows with increasing thickness of the thin film layer until saturation is reached. The modeling of such growth processes has been done by Barabasi and Stanley [1], Kardar, Parisi, and Zhang [3], Linz et al. [4], and Raible et al. [8,9].

We assume a particle beam perpendicular to the substrate (cf. Fig. 1) and denote by

$$u(x,t) := H(x,t) - Ft \tag{1.1}$$

the height profile where $H(x,t)$ is the absolute height and F refers to the rate of deposition. Then, in case of low energy deposition, the height profile can be shown to satisfy the following nonlinear evolution equation

$$\frac{\partial u}{\partial t} = a_1\Delta u + a_2\Delta^2 u + a_3\Delta(\nabla u)^2 + a_4(\nabla u)^2 \tag{1.2}$$

*Institute of Mathematics, University of Augsburg, D-86159 Augsburg, Germany

This work was supported by the German National Science Foundation (DFG) within the DFG-funded Collaborative Research Field SFB 438.

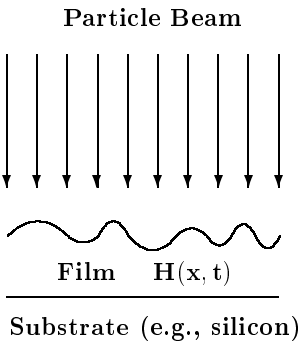

Figure 1. Amorphous growth of thin films by molecular beam epitaxy.

in $Q := \Omega \times [0,\infty)$, $\Omega := \prod_{\nu=1}^{d}[0,L_\nu]$, with either periodic or homogeneous Neumann boundary conditions on $\Gamma := \partial\Omega$ and an appropriate initial condition $u(x,0) = u^0(x)$, $x \in \Omega$. Here, $a_1 = -Gb$ and $a_4 = Gb^2$ where G is the mean surface growth and b reflects the typical range of interatomic and van der Waals forces between the surface atoms and the impinging particles. Moreover, a_2 and a_3 are related to surface diffusion (see, e.g., [10]) with a_3 given by $a_3 = -G\ell^2/8$ where ℓ^2 represents the mean square of the diffusion length (cf. [8]).

If b is small, the fourth term on the right-hand side of (1.2) can be neglected. Consequently, in this case (1.2) can be written as

$$\frac{\partial u}{\partial t} = \Delta\left(a_1 u + a_2 \Delta u + f(u)\right) \tag{1.3}$$

where $f(u) := a_3(\nabla u)^2$. We remark that the model has to be modified, if the particle beam is not impinging perpendicularly to the substrate. In this case, other techniques, as for instance level set methods, have to be used for simulation purposes (cf., e.g., [6,7]).

In the one-dimensional case, i.e., $d = 1$ and $\Omega := [0,L]$, the existence of a solution

$$u \in C\left([0,T], L^2([0,L])\right) \cap L^2\left([0,T], H^2([0,L])\right)$$

with initial data $u^0 \in L^2([0,L])$ has been proved in [2]. Moreover, in case $\Omega := [0,L]^d$, $d \leqslant 3$, it can be shown that for some finite time interval $[0,t^*]$, $t^* > 0$, the solution exhibits some unexpected linear behavior: We denote by $\lambda_i \in \mathbb{R}$ with $\lambda_i \geqslant \lambda_{i+1}$ and φ_i, $i \in \mathbb{N}$, the eigenvalues and associated eigenfunctions of the linear operator representing the linearization of the right-hand side in (1.3) and by

$$X^+, X^{++} \subset X := \left\{ u \in L^2(\Omega) \;\middle|\; \int_\Omega u \,\mathrm{d}x = 0 \right\}$$

the linear spaces spanned by the eigenfunctions φ_i associated with eigenvalues in the intervals

$$(\gamma_1\lambda_1, \gamma_2\lambda_1) \quad \text{and} \quad (\gamma_2\lambda_1, +\infty), \quad 0 \ll \gamma_1 < \gamma_2 < 1.$$

Then, if $Y := X^+ \oplus X^{++}$ and $\bar{u}^0 := |\Omega|^{-1} \int_\Omega u^0 \, dx$, the following result can be verified:

Theorem 1.1 (cf. [2]). *Assume $u^0 \in H^3([0,L]^d)$, $d \leqslant 3$, with $\|u^0\| \leqslant CL^{2+d/2-r}$, $r > 0$. Then, there exists $t^* > 0$ such that the solution $u = u(x,t)$, $x \in [0,L]^d$, $t \in [0,t^*)$, of (1.3) stays with probability close to 1 in a vicinity of the dominant subspace $\bar{u}^0 + Y$ until at $t = t^*$ it leaves a ball $B_R(0)$ with radius $R \leqslant CL^{2+d/2-r}$. The solution exhibits a spinodal decomposition with patterns of order $O(1)$.*

The preceding result, which has been established based on a spectral Galerkin approximation of the solution, strongly suggests to use spectral elements in the numerical solution of (1.3) as long as linear behavior prevails and to switch to some other discretization technique when nonlinear behavior sets in. We consider a combined spectral element/finite element approach. In particular, in section 2 we will outline a spectral Galerkin method whereas in section 3 we will elaborate on a finite element technique that is based on the reformulation of (1.3) as an equivalent system of two 2nd order PDEs and thus allows the use of C^0-elements for discretization. Finally, in section 4 we will present the results of numerical simulations of the epitaxial growth of thin ZrAlCu films.

2. THE SPECTRAL ELEMENT METHOD

We set $V := H^2_{per}(\Omega)$ in case of periodic boundary conditions and $V := H^2(\Omega)$ for homogeneous Neumann boundary conditions, and we denote by $u^m \in V$ an approximation of the solution u of (1.3) at time level $t = t_m$. Then, if we discretize (1.3) in time by the fully implicit backward Euler scheme, we arrive at the variational equation

$$\int_\Omega u^m \chi \, dx = \int_\Omega u^{m-1} \chi \, dx + \tau_m \int_\Omega (a_1 u^m + a_2 \Delta u^m + f(u^m)) \Delta\chi \, dx, \quad \chi \in V \tag{2.1}$$

where $\tau_m := t_m - t_{m-1}$.

We consider the first N eigenvalues λ_i of $-\Delta$ and denote by $V_N \subset V$ the subspace spanned by the associated orthonormal eigenfunctions φ_i, $1 \leqslant i \leqslant N$, i.e.,

$$V_N := \{\varphi_i \mid 1 \leqslant i \leqslant N\}, \quad \int_\Omega \varphi_i \varphi_j \, dx = \delta_{ij}, \quad 1 \leqslant i, j \leqslant N.$$

The spectral Galerkin approximation

$$u^{m,*} = \sum_{i=1}^{N} u_i^m \varphi_i \tag{2.2}$$

of the solution u^m of (2.1) then results in the following nonlinear system of equations

$$\begin{aligned} g_i(\mathbf{u}^m) \;:=\; & (1 + a_1\tau_m\lambda_i - a_2\tau_m\lambda_i^2)u_i^m \\ & + \;\tau_m\lambda_i \int\limits_\Omega f\left(\sum_{k=1}^N u_k^m\varphi_k\right)\varphi_i \,\mathrm{d}x - u_i^{m-1} = 0, \quad 1 \leqslant i \leqslant N \end{aligned} \tag{2.3}$$

where $\mathbf{u}^m := (u_1^m, \ldots, u_N^m)^T$. Using $\mathbf{u}^{m,0} := \mathbf{u}^{m-1}$ as a startiterate, (2.4) is solved by Newton's method

$$\begin{aligned} J_g(\mathbf{u}^{m,\nu})\delta_{\mathbf{u}^m}^\nu &= -g(\mathbf{u}^{m,\nu}) \\ \mathbf{u}^{m,\nu+1} &= \mathbf{u}^{m,\nu} + \delta_{\mathbf{u}^m}^\nu, \qquad \nu = 0, 1, 2, \ldots \end{aligned} \tag{2.4}$$

where J_g is the Jacobian of the nonlinear mapping g.

The disadvantage of (2.5) is that we have to solve a linear system with a densely populated $N \times N$ coefficient matrix. This can be avoided by using the method of successive approximations

$$\int\limits_\Omega u^{m,\nu}\chi \,\mathrm{d}x = \int\limits_\Omega u^{m-1}\chi \,\mathrm{d}x + \tau_m + \int\limits_\Omega (a_1 u^{m,\nu} + a_2\Delta u^{m,\nu} + f(u^{m,\nu-1}))\Delta\chi \,\mathrm{d}x, \;\; \chi \in V \tag{2.5}$$

where the startiterate $u^{m,0} \in V$ is determined by means of the semiimplicit backward Euler scheme

$$\int\limits_\Omega u^m\chi \,\mathrm{d}x = \int\limits_\Omega u^{m-1}\chi \,\mathrm{d}x + \tau_m \int\limits_\Omega (a_1 u^m + a_2\Delta u^m + f(u^{m-1}))\Delta\chi \,\mathrm{d}x, \quad \chi \in V. \tag{2.6}$$

Together with the spectral Galerkin approximation (2.2), the fixed point iteration (2.5) yields the equations

$$u_i^{m,\nu} = (u_i^{m-1} - \tau_m\lambda_i f_i^{m,\nu-1})/(1 + a_1\tau_m\lambda_i - a_2\tau_m\lambda_i^2), \quad 1 \leqslant i \leqslant N \tag{2.7}$$

where $f_i^{m,\nu-1} := \int_\Omega f\left(\sum_{k=1}^N u_k^{m,\nu-1}\varphi_k\right)\varphi_i \,\mathrm{d}x$, $1 \leqslant i \leqslant N$.

The coefficients $f_i^{m,\nu-1}$ in (2.7) can be efficiently computed using the Fast Fourier Transform in case of periodic boundary conditions and the Fast Cosine Transform for homogeneous Neumann boundary conditions with respect to an equidistant grid $\{x = (x_{\nu_1}, \ldots, x_{\mu_d})^T \mid 1 \leqslant \mu_d \leqslant M,\ 1 \leqslant k \leqslant d\}$ of $\Omega = \prod_{k=1}^d [0, L_k]$. In order to avoid aliasing effects, we must choose $M > N$. If we choose $M > 2N$, then all coefficients $f_i^{m,\nu-1}$ are computed exactly, since f is a polynomial of degree 2. For each iterate $\mathbf{u}^{m,\nu} \in \mathbb{R}^N$ we compute the defect $\mathbf{d}^{m,\nu}$ according to

$$d_i^{m,\nu} = (1 + a_1\tau_m\lambda_i - a_2\tau_m\lambda_i^2)u_i^{m,\nu} - u_i^{m-1} + \tau_m\lambda_i f_i^{m,\nu}, \quad 1 \leqslant i \leqslant N \tag{2.8}$$

and stop the iteration, if for a prespecified tolerance 'tol' there holds

$$\|\mathbf{d}^{m,\nu}\| := \left(\sum_{i=1}^{N}(d_i^{m,\nu})^2\right)^{1/2} \leqslant \text{tol} \tag{2.9}$$

or

$$\|\mathbf{d}^{m,\nu}\| > \|\mathbf{d}^{m,\nu-1}\|. \tag{2.10}$$

In the first case, we accept $\mathbf{u}^{m,\nu}$ as an approximation of u at $t = t_m$. On the other hand, if (2.10) applies, we choose $\mathbf{u}^{m,\nu-1}$ as a startiterate for Newton's method (2.5). However, if (2.10) occurs at $n_{\max}$ consecutive time levels, this will serve as an indicator that nonlinear dynamics has set in, i.e., $t_m > t^*$, and we switch to the finite element method described in the following section.

The spectral Galerkin approximation goes along with an automatic step size control in time based on extrapolation techniques using the semiimplicit backward Euler method (cf. (2.6)) as the basis scheme and the trapezoidal rule

$$\int_\Omega \tilde{u}^m \psi \,\mathrm{d}x = \int_\Omega u^{m-1}\,\mathrm{d}x + \frac{\tau_m}{2}\int_\Omega \big[a_1(\tilde{u}^m + u^{m-1}) + a_2\Delta(\tilde{u}^m + u^{m-1}) + (f(u^m) + f(u^{m-1}))\big]\Delta\psi\,\mathrm{d}x, \quad \psi \in V \tag{2.11}$$

as the reference scheme which results in

$$\tilde{u}_i^m = u_i^{m-1} - \frac{\tau_m}{2}\big[a_1\lambda_i(\tilde{u}_i^m + u_i^{m-1}) - a_2\lambda_i^2(\tilde{u}_i^m + u_i^{m-1}) - \lambda_i(f_i^m + f_i^{m-1})\big], \quad 1 \leqslant i \leqslant N. \tag{2.12}$$

The trapezoidal rule allows an interpretation as an additive correction to the backward Euler scheme, so that $\boldsymbol{\eta}^m := \tilde{\mathbf{u}}^m - \mathbf{u}^m$ can be easily computed by means of

$$\eta_i^m = \frac{\tau_m\big[(a_1\lambda_i - a_2\lambda_i^2)(\tilde{u}_i^m - u_i^{m-1}) - \lambda_i(f_i^m - f_i^{m-1})\big]}{2(1 + a_1\tau_m\lambda_i - a_2\tau_m\lambda_i^2)}, \quad 1 \leqslant i \leqslant N. \tag{2.13}$$

However, we have additionally to take into account the error caused by the discretization in space. For the spectral element method, this is basically the error due to the negligence of those modes that are relevant for the exact computation of the nonlinearities, and thus is given by

$$e_{\mathbf{u}^m} = \sum_{N<i\leqslant 2N} \tau_m\lambda_i f_i^m / \left(1 + a_1\tau_m\lambda_i - a_2\tau_m\lambda_i^2\right). \tag{2.14}$$

We note that the coefficients f_i^m, $i > N$, have already been determined in the course of the computation of u_i^m (see above) so that $e_{\mathbf{u}^m}$ is cheaply available. With respect to the tolerance 'tol', the prediction for a new time step size $\tilde{\tau}^m$ is then given by

$$\tilde{\tau}_m := \sqrt{(\sigma_d\,\text{tol}\|\tilde{\mathbf{u}}^m\| - |e_{\mathbf{u}^m}|)/\|\boldsymbol{\eta}^m\|} \tag{2.15}$$

where $\|\cdot\|$ stands for the Euclidean norm in $\mathbb{R}^N$ and $\sigma_d < 1$ is a weighting factor depending on the spatial dimension of the problem (e.g., $\sigma_d = 1/(d+1)$). In practice, we monitor the time step size selection by means of the criterion

$$\frac{\|\boldsymbol{\eta}^m\| + (\sigma_d^{-1} - 1)\,|e_{\mathbf{u}^m}|}{\|\tilde{\mathbf{u}}^m\|} \leqslant \text{tol}. \tag{2.16}$$

If (2.16) is satisfied, we proceed to the next time level with step size $\tau_{m+1} := \tilde{\tau}_m$. Otherwise, we repeat the previous time step with the new step size $\tau_m := \tilde{\tau}_m$ (see [5] for details).

3. THE FINITE ELEMENT METHOD

The nonlinear parabolic PDE (1.3) is 4th order in space. Consequently, a conforming finite element approach would require C^1-elements and thus lead to a significantly large number of nodal points. Instead, we reformulate (1.3) as a system of two 2nd order equations

$$\frac{\partial u}{\partial t} = \Delta w \tag{3.1}$$

$$w = a_1 u + a_2 \Delta u + f(u) \tag{3.2}$$

which allows us to use C^0-elements. Indeed, the variational formulation of (3.1), (3.2) is given by

$$\int_\Omega \frac{\partial u}{\partial t}\psi \,\mathrm{d}x + \int_\Omega \nabla w \cdot \nabla \psi \,\mathrm{d}x = 0, \quad \psi \in H^1(\Omega)$$

$$\int_\Omega w\psi \,\mathrm{d}x - a_1 \int_\Omega u\psi \,\mathrm{d}x + a_2 \int_\Omega \nabla u \cdot \nabla \psi \,\mathrm{d}x - \int_\Omega f(u)\psi \,\mathrm{d}x = 0, \quad \psi \in H^1(\Omega).$$

Since the finite element approach is to be performed when the nonlinear dynamics prevails, for discretization in time we rely on the fully implicit backward Euler scheme

$$\int_\Omega u^m \psi \,\mathrm{d}x + \tau_m \int_\Omega \nabla w^m \cdot \nabla \psi \,\mathrm{d}x = \int_\Omega u^{m-1}\psi \,\mathrm{d}x, \quad \psi \in H^1(\Omega) \tag{3.3}$$

$$\begin{aligned} \int_\Omega w^m \psi \,\mathrm{d}x - \tau_m a_1 \int_\Omega u^m \psi \,\mathrm{d}x + \tau_m a_2 \int_\Omega \nabla u^m \cdot \nabla \psi \,\mathrm{d}x \\ - \int_\Omega f(u^m)\psi \,\mathrm{d}x = \int_\Omega w^{m-1}\psi \,\mathrm{d}x, \quad \psi \in H^1(\Omega). \end{aligned} \tag{3.4}$$

For discretization in space we consider a nested hierarchy of simplicial triangulations $(\mathscr{T}_k)_{k=0}^{\ell}$, i.e., $\mathscr{T}_0 \subset \mathscr{T}_1 \subset \ldots \subset \mathscr{T}_\ell$, and denote by $S_1(\Omega;\mathscr{T}_k)$, $0 \leqslant k \leqslant \ell$, the

associated finite element space of continuous, piecewise linear finite elements with respect to $\mathscr{T}_k$. Then, on the finest grid $\mathscr{T}_\ell$ the Galerkin approximation of (3.3), (3.4) reads as follows

$$\int_\Omega u_\ell^m \psi_\ell \, dx + \tau_m \int_\Omega \nabla w_\ell^m \cdot \nabla \psi_\ell \, dx = \int_\Omega u_\ell^{m-1} \psi_\ell \, dx, \quad \psi_\ell \in S_1(\Omega, \mathscr{T}_\ell) \tag{3.5}$$

$$\begin{aligned} \int_\Omega w_\ell^m \psi_\ell \, dx - \tau_m a_1 \int_\Omega u_\ell^m \psi_\ell \, dx + \tau_m a_2 \int_\Omega \nabla u_\ell^m \cdot \nabla \psi_\ell \, dx \\ - \int_\Omega f(u_\ell^m) \psi_\ell \, dx = \int_\Omega w_\ell^{m-1} \psi_\ell \, dx, \quad \psi_\ell \in S_1(\Omega, \mathscr{T}_\ell). \end{aligned} \tag{3.6}$$

We numerically solve (3.5),(3.6) by a Newton multigrid method, i.e., on the finest grid we apply Newton's method to (3.5), (3.6) and solve the resulting linear system in the Newton increments by a linear multigrid method with respect to the given hierarchy of triangulations. To be more specific, given $u_\ell^{m,\nu}$, $w_\ell^{m,\nu} \in S_1(\Omega, \mathscr{T}_\ell)$, we compute

$$\begin{aligned} u_\ell^{m,\nu+1} &= u_\ell^{m,\nu} + \delta_{u_\ell}^{m,\nu}, \quad \nu = 0, 1, 2, \ldots \\ w_\ell^{m,\nu+1} &= w_\ell^{m,\nu} + \delta_{w_\ell}^{m,\nu}, \quad \nu = 0, 1, 2, \ldots \end{aligned}$$

where $(\delta_{u_\ell}^{m,\nu}, \delta_{w_\ell}^{m,\nu}) \in S_1(\Omega, \mathscr{T}_\ell)^2$ is the solution of the linear system

$$\begin{aligned} \int_\Omega \delta_{u_\ell}^{m,\nu} \psi_\ell \, dx + \tau_m \int_\Omega \nabla \delta_{u_\ell}^{m,\nu} \cdot \nabla \psi_\ell \, dx = \int_\Omega u_\ell^{m-1} \psi_\ell \, dx \\ - \int_\Omega u_\ell^{m,\nu} \psi_\ell \, dx - \tau_m \int_\Omega \nabla w_\ell^{m,\nu} \cdot \nabla \psi_\ell \, dx, \quad \psi_\ell \in S_1(\Omega, \mathscr{T}_\ell) \end{aligned} \tag{3.7}$$

$$\begin{aligned} \int_\Omega \delta_{w_\ell}^{m,\nu} \psi_\ell \, dx - a_1 \tau_m \int_\Omega \delta_{u_\ell}^{m,\nu} \psi_\ell \, dx + a_2 \tau_m \int_\Omega \nabla \delta_{u_\ell}^{m,\nu} \cdot \nabla \psi_\ell \, dx \\ - \tau_m \int_\Omega f'(u_\ell^{m,\nu}) \delta_{u_\ell}^{m,\nu} \psi_\ell \, dx = \int_\Omega w_\ell^{m-1} \psi_\ell \, dx - \int_\Omega w_\ell^{m,\nu} \psi_\ell \, dx + a_1 \tau_m \int_\Omega u_\ell^{m,\nu} \psi_\ell \, dx \\ - a_2 \tau_m \int_\Omega \nabla u_\ell^{m,\nu} \cdot \nabla \psi_\ell \, dx + \tau_m \int_\Omega f(u_\ell^{m,\nu}) \psi_\ell \, dx, \quad \psi_\ell \in S_1(\Omega, \mathscr{T}_\ell). \end{aligned} \tag{3.8}$$

The linear multigrid method applied to (3.7), (3.8) is implemented using standard multigrid intergrid transfers and ILU both as a smoother on all levels $1 \leqslant k \leqslant \ell$ as well as an iterative solver on level $k = 0$.

Again, we use an adaptive time step size selection similar to the one described in the previous section except that we compute $e_{\mathbf{u}^m}$ by means of a residual based a posteriori error estimator (see [5] for details).

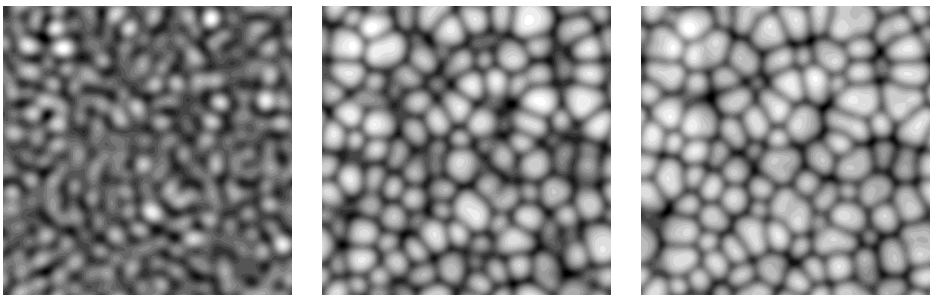

Figure 2. Computed patterns for different film thicknesses.

4. SIMULATION RESULTS

We have used the combined spectral element/finite element approximation to compute the morphology of the surface growth of thin *ZrAlCu* films. In case $\Omega := [0,1]^2$, we started from randomly chosen initial data u^0 using different numbers of Fourier modes ($N = 125, 200$, and 250) in the spectral Galerkin approach resp. different hierarchies of triangulations $(\mathscr{T}_k)_{k=0}^{\ell}$ (with $h_\ell = 1/200, 1/256$ and $1/400$) in the finite element approximation.

Numerical experience shows that in the initial time interval, where linear behavior is dominant, the method of succesive approximations (2.5) only requires very few iterations ($\mathrm{tol} = 10^{-4}$). The closer we get to t^*, the more iterations have to performed. We switch to the finite element method, if (2.5) is observed for $n_{\max} = 3$ subsequent time levels. In the Newton multigrid approach based on the finite element discretization, a different behavior can be seen. At the beginning, several outer Newton iterations are required to determine the solution at the next time level. However, the closer we get to the equilibrium state, the fewer Newton iterations are necessary.

Figure 2 illustrates the computed patterns for a film thickness of 100*nm* (left), 360*nm* (middle), and 480*nm* (right) (in case $N = 250$ resp. $h_\ell = 1/400$). We note that the computed patterns are in very good agreement with experimental data obtained by TEM (Transmission Electron Microscopy) (cf. [8]). We have compared the performance of our approach with the finite difference method used in [8,9]. For that purpose, both methods have been implemented on the same platform (DEC Alpha au/128).

Table 1.
Comparison of CPU times.

Spectral/Finite El.			Finite Differences		
u_{125}	u_{200}	u_{250}	$\hat{u}_{200}$	$\hat{u}_{256}$	$\hat{u}_{400}$
37	313	321	21	103	1621

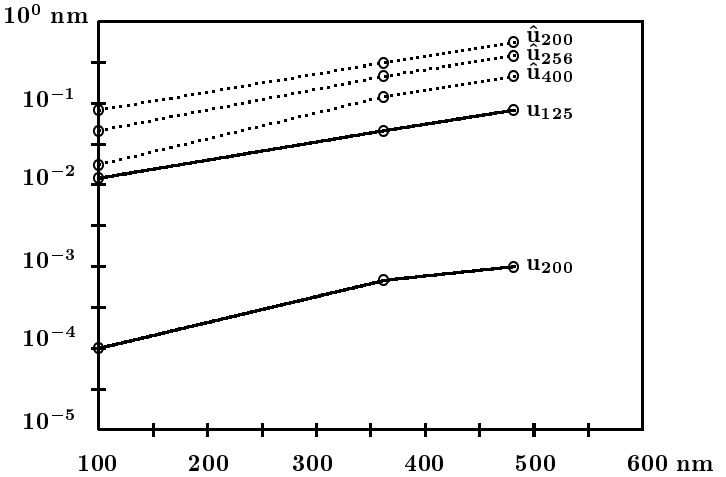

Figure 3. Deviation from the reference solution.

Table 1 contains the CPU times necessary to obtain a film thickness of 480 nm where u_{125}, u_{200}, and u_{250} refer to the spectral element/finite element method with $N = 125$, $N = 200$, $N = 250$ ($h_\ell = 1/200$, $h_\ell = 1/256$, $h_\ell = 1/400$) whereas $\hat{u}_{200}$, $\hat{u}_{256}$ and $\hat{u}_{400}$ represent the finite difference method with respect to an equidistant grid in space with step sizes $h = 1/200$, $h = 1/256$, and $h = 1/400$. Moreover, using u_{250} as a reference solution, Figure 3 displays the deviation of u_{125}, u_{200}, and $\hat{u}_{200}$, $\hat{u}_{256}$, $\hat{u}_{400}$ from the reference solution.

Both, Table 1 and Figure 3 clearly illustrate the superiority of the spectral element/finite element technique which allows to compute approximations more accurately in less computational time.

REFERENCES

1. A. L. Barabasi and H. E. Stanley, *Fractal Concepts in Surface Growth*. Cambridge Univ. Press, Cambridge, 1995.
2. D. Blömker, *Stochastic Partial Differential Equations and Surface Growth*. Wissner, Augsburg, 2000.
3. M. Kardar, G. Parisi, and Y.-C. Zhang, Dynamic scaling of growing interfaces. *Phys. Rev. Lett.* (1986) **56**, 889 – 892.
4. S. J. Linz, M. Raible, and P. Hänggi, Stochastic field equation for amorphous surface growth. *Lecture Notes in Physics* (2000) **557**, 473 – 483.
5. E. M. Nash, *Finite-Elemente und Spektral-Galerkin Verfahren zur numerischen Lösung der Cahn-Hilliard Gleichung und verwandter nichtlinearer Evolutionsgleichungen*. Shaker, Aachen, 2001.
6. Ch.-D. Nguyen and R. H. W. Hoppe, Amorphous surface growth via a level set approach, submitted to *Nonlinear Analysis: Theory, Methods, and Applications* (2002).

7. Ch.-D. Nguyen and R. H. W. Hoppe, A nonlinear semigroup approach to weak solutions of evolution equations describing amorphous surface growth of thin film depositions, submitted to *Nonlinear Analysis: Theory, Methods, and Applications* (2002).
8. M. Raible, S. G. Mayr, S. J. Linz, M. Moske, P. Hänggi, and K. Samwer, Amorphous thin film growth: theory compared with experiment. *Europhys. Lett.* (2000) **50**, 61 – 67.
9. M. Raible, S. J. Linz, and P. Hänggi, Amorphous thin film growth: Minimal deposition equation. *Phys. Rev. E* (2000) **62**, 1691 – 1705.
10. D. E. Wolf and J. Villain, Growth with surface diffusion. *Europhys. Lett.* (1990) **13**, 389 – 394.